A High Voltage, Constant Current Stimulator for Electrocutaneous Stimulation Through Small Electrodes

Christopher J. Poletto* and Clayton L. Van Doren

Abstract—A high-voltage stimulator has been designed to allow transcutaneous stimulation of tactile fibers of the fingertip. The stimulator's output stage was based upon an improved Howland current pump topology, modified to allow high load impedances and small currents. The compliance voltage of approximately 800 V is achieved using commercially available high-voltage operational amplifiers. The output current accuracy is better than $\pm 5\%$ over the range of 1 to 25 mA for 30 μs or longer pulses. The rise time for square pulses is less than 1 μs. High-voltage, common-mode, latch-up power supply problems and solutions are discussed. The stimulator's input stage is optically coupled to the controlling computer and complies with applicable safety standards for use in a hospital environment. The design presented here is for monophasic stimulation only, but could be modified for biphasic stimulation.

Index Terms— Common mode latch-up, current source, electrocutaneous stimulation, electrode/skin interface, electrotactile stimulation, high voltage, pain.

I. INTRODUCTION

ELECTROCUTANEOUS (electrotactile) stimulation is the evocation of tactile (touch) sensations within the skin by passing a local electric current through the skin, usually via an electrode placed on the skin surface. Many authors have suggested the use of electrocutaneous stimulation in sensory substitution systems for blind or deaf persons and for users of prostheses. Specific applications include reading aids [1], visual prostheses (tactile visual substitution, e.g., [2]–[4]), and mobility aids [5] for the blind, as well as auditory prostheses (e.g., [6]–[9]). Electrocutaneous stimulation also has been used to improve the utility of upper extremity (e.g., [10]–[18]) and lower extremity (e.g., [19]–[21]) prostheses for amputees. Subdermal electrocutaneous stimulation has been used to provide sensory feedback to users of an upper extremity neuroprosthesis (e.g., [22]). Electrocutaneous arrays on the forehead have been used to help people with advanced cases of Hansen's disease (leprosy) to perform detailed manual tasks with reduced chance of injury [23].

*C. J. Poletto is with the Department of Biomedical Engineering, Case Western Reserve University, 2500 MetroHealth Dr., Cleveland, OH 44109-1998 USA (e-mail: cxp17@po.cwru.edu).
C. L. Van Doren is with the Department of Orthopaedics, Case Western Reserve University, Cleveland, OH 44109-1998 USA.

Electrocutaneous/electrotactile stimulation may also be useful in virtual reality, telerobotics and telepresence. Electrical stimulation of the fingertip could be used to communicate tactile information to the user of a telerobotic manipulator or similar device. Presenting detailed spatial information, such as surface texture, would require the use of a dense array of many small electrodes. In all the example applications cited above, however, the stimulation was delivered through electrodes at least 3 mm in diameter (except in the cases of [1] where a 0.3-mm-diameter electrode was tried and rejected and [22] where a small, subdermal electrode was used successfully). Our initial investigations as well as reports from several other authors (e.g., [1], [8], [9], and [24]) indicate that a fundamental limitation on the use of small electrodes is that the dynamic range, the range of stimulus intensities above sensation threshold but below the pain threshold, is more limited with smaller electrodes (e.g., 1-mm diameter). We have designed a high voltage, controlled current stimulator to aid in our investigation of this phenomenon. Conventional electrical stimulators are designed to stimulate through electrodes at least 3 mm in diameter and typically have compliance voltages of 120 V [25] or less. The impedance of the skin renders these stimulators inadequate for use with smaller electrodes, especially on the finger tip where the outer layer of skin, the stratum corneum, is much thicker than most other areas on the body (600-μm versus 15-μm thick [26]). Other, higher voltage stimulators (500-V maximum compliance voltage) have been presented (e.g., [1]), but they were not designed to offer the precise current or timing control required for our research. Also, 500 V compliance may still not be sufficient to deliver the full dynamic range of stimulation through the small electrodes we intend to use. We have, therefore, designed our own constant current stimulator capable of precise control of stimulus pulse timing and intensity over a wider range of load impedances than previously available.

A. Device Specifications: Output Stage

We require a stimulator that can deliver combinations of long (1 ms or longer), low current ($<$1 mA) and short (30 μs), high current (up to 25 mA) pulses through a 1-mm-diameter electrode on the finger tip. Because we are designing a laboratory research device, and because short pulse widths may be required, rise times need to be short ($<$2 μs) so that the charge contained in the short pulses will be as close to the ideal as possible (ideal charge $= PW \times I$).
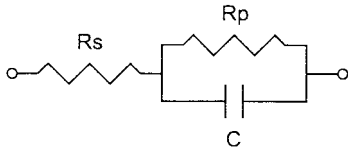
Fig. 1. First-order electrical model of the skin, where R_S represents the bulk tissue resistance, R_P and C represent the resistive and reactive components of the electrode/skin interface. For a 1-mm-diameter Ag/AgCl electrode on a well-hydrated, conditioned fingertip, approximate values are: $R_S = 2$ kΩ, $C = .42$ nF, with R_P ranging from 10 kΩ to 320 kΩ, depending on current.
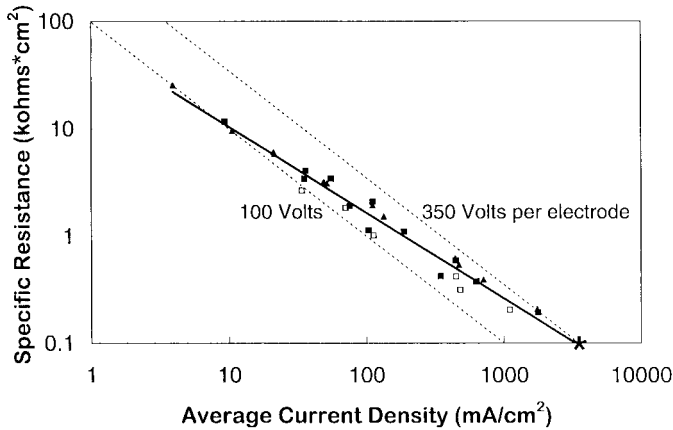

Fig. 2. Specific parallel resistance, r_p, of the finger tip skin plotted as a function of current density, J, for three subjects and four electrodes (Ag/AgCl electrodes 1-, 2-, 4-, 8-mm diameter). Symbols denote subjects. Dashed lines indicate 100 V and 350 V equipotential lines of required driving voltage for each electrode/skin interface. The solid line represents a power function of the form $r_p = 65.7 \cdot J^{-0.80}, R^2 = 0.97$.

We can estimate the voltages required to drive the desired currents though the fingertip using a simple, first-order model of the skin impedance consisting of a parallel RC network in series with a smaller resistor, as shown in Fig. 1 (e.g., [27]–[31]). The series resistance, which can be thought to represent the bulk tissue resistance, is generally small, ~2 kΩ (as measured in our lab, and well within the range reported elsewhere e.g., [27]–[30]). The value of the capacitance varies as a function of electrode surface area. We measured this capacitance for 1-, 2-, 4-, and 8-mm diameter Ag/AgCl electrodes (Neuromedical Supplies Inc.; Herndon, VA) and found it to range from 0.4 nF (1 mm) to 5.2 nF (8 mm). The parallel resistance, R_p, represents the largest portion of the DC impedance and its value depends strongly on current density. The values we measured using a 1-mm Ag/AgCl disk electrode ranged from 10 kΩ to 320 kΩ for currents ranging from 25 mA down to 0.5 mA, respectively. If R_p is assumed to scale inversely with electrode surface area, then it is useful to generalize across electrode diameters by computing the specific resistance, r_p. The concept of specific resistance is common in the materials science literature, but has not been used before to characterize an electrode/skin interface. Fig. 2 shows specific resistance, measured through four electrode sizes (1-, 2-, 4-, and 8-mm diameter) on the fingertips of three subjects, plotted against average current density. These values were for skin that had been cleaned with alcohol, well hydrated with tap water, and stimulated for several minutes
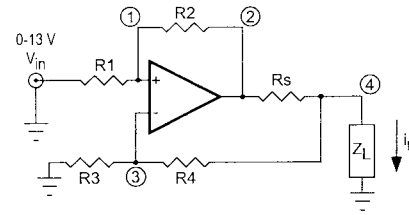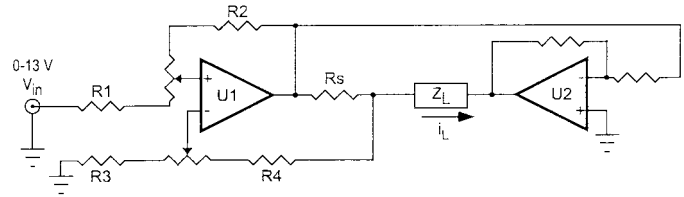
Fig. 3. Simplified schematic of the improved Howland current pump configuration used in the stimulator output stage. (a) Howland current pump by itself with node numbers indicated. (b) Current pump in bridge configuration. U1 is the master op-amp; U2 is the slave op-amp and is configured as a unity inverter. $R_1 = R_3 = 5$ kΩ, $R_2 = 10$ kΩ, $R_s = 1$ kΩ, $R_4 = 9$ kΩ. Z_L represents the load impedance.

prior to impedance measurement. If these conditions were not met, measured impedances were considerably higher. Note that all of these measurements were made using a cathodic disk electrode on the fingertip and a large flexible gel electrode on the back of the finger or hand. The impedances would be much greater if the surface area of the return was also small, as we intend to use in some of our experiments. We also plan to stimulate through electrodes smaller than 1 mm, in which case, the impedance will be even higher. Although the impedance data we present here is for Ag/AgCl electrodes, we also will use stainless steel electrodes in cases where significant unbalanced anodic current is anticipated. Based on preliminary data, stainless steel electrodes present a higher impedance interface than do Ag/AgCl electrodes. To be safe, we designed the stimulator to be able to stimulate at the estimated maximum tolerable current (7 mA) through a 0.5-mm-diameter anode and cathode. In this case, almost 700 V would be required to produce 7 mA of current ($V = I \cdot 2 \cdot R = 2 \cdot J \cdot r_p \approx 680$V with $J = 7$ mA$/.002$ cm$^2 = 3565$ mA/cm^2 and r_p estimated from the equation in Fig. 2 legend, *).

II. METHODS

A. The Output Stage

Several possible current source output stage topologies were considered. We elected to use an op-amp-based output stage given the commercial availability of high-voltage op-amps with excellent slew rates and up to 450 V outputs. Since we required a compliance voltage almost twice the maximum output voltage of available op-amps, we needed a current source circuit that used a grounded load so that a bridge configuration could be employed to double the compliance voltage. The improved Howland current pump in a bridge (master/slave) configuration was an appropriate choice. The topology of the typical improved Howland current pump is shown in Fig. 3(a), while the bridge configuration is given

in Fig. 3(b). The master op-amp circuitry performs a voltage to current conversion. The current through the load creates a differential voltage across the sense resister, R_s. This voltage is fed back to the inputs and is subtracted (summed at the inverting input) from the voltage applied at the input to R_1, yielding a differential voltage. Since the op-amp does not tolerate any net differential voltage at its inputs, it ensures that the voltage across the sense resistor equals the input voltage. We can calculate the load current and specify component value relationships, through the following node-voltage analysis:

$$\frac{v_{\text{in}} - v_1}{R_1} + \frac{v_2 - v_1}{R_2} = 0 \quad i_L = \frac{v_2 - v_4}{R_s} + \frac{v_3 - v_4}{R_4}$$
$$\frac{v_4 - v_3}{R_4} - \frac{v_3}{R_3} = 0 \quad v_3 = v_1. \tag{1}$$

Performing the algebra and solving for i_L yields

$$i_L = \frac{-v_{\text{in}}\left(\frac{R_2}{R_1 R_s}\right)}{1 - \varepsilon}$$

where

$$\varepsilon = Z_L\left(\frac{R_2 R_3 - R_1 R_s - R_1 R_4}{R_1 R_s (R_3 + R_4)}\right). \tag{2}$$

The typical textbook analysis of the improved Howland current pump assumes that the sense resistor, R_s is very small compared to the resistors in the inverting and noninverting feedback pathways and that the load impedance is much lower than that of the feedback pathways (e.g., [32] and [33]). Given these assumptions, the output impedance of the current source is maximized if the ratios R_2/R_1 and R_4/R_3 are exactly matched. In this case, ε in (2) reduces to $\varepsilon = (-Z_L)/(R_3 + R_4)$, which is negligible if the load impedance is small compared to the feedback resistors. This leads to the expression generally given for the load current

$$i_L = i_s = -v_{\text{IN}} \cdot \frac{R_2}{R_1 \cdot R_s}. \tag{3}$$

This strategy is inappropriate, however, when the load impedance is substantial, as in our case, since the feedback resistors would have to be extremely large. Although SPICE simulations work well with large feedback resistors (1 MΩ), the practical use of such resistors typically leads to amplifier oscillation. Another problem with the textbook approach is that we wish to control small currents at high voltages. The use of a small sense resistor could diminish the feedback voltage to the level of the thermal noise of the large resistors and, thus, seriously degrade the accuracy of the current control.

The solution is to use R_s large enough to provide adequate feedback, and reduce the size of the feedback resistors. When $R_3 = R_1$ and $R_2 = R_s + R_4$, the ε term in (2) disappears and the load current is given by (3), as desired. Note that the derivation of this equation, unlike the textbook case, does not depend on the assumption that the load impedance is much lower than the feedback impedance and that, therefore,

practically no current flows in the noninverting feedback path. In fact, because the load voltage no longer appears in the equation, current regulation can be maintained even when the load impedance is much greater than the feedback resistance as long as the amplifier is operating in its linear range.

Our modifications accommodate larger load impedances but maximum output current is reduced in two ways: 1) The lower the feedback resistors, the higher the current is through those pathways. Since all current must be sourced by the op-amp, and since the op-amp has a maximum safe current output, this increased feedback current lowers the current that is available to flow through the load. 2) By increasing the value of R_s, we increase the voltage dropped across it, thereby decreasing the compliance voltage. As stated above, we would like the value of R_s to be as large as practical in order to increase accuracy, but we would also like it to be as small as possible so as not to limit compliance voltage. The R_s value of 1 kΩ represents a compromise which allows current regulation to within about 50 μA (5% of 1 mA), while decreasing the compliance voltage no more than 25 V. Overall, our initial measurements indicate that the available current is still more than enough to span the dynamic ranges available for the 1- to 8-mm-diameter electrodes we intend to use.

The saturation voltage of the op-amp determines the maximum voltage that can be applied to a given load impedance. To extend the attainable load voltage, we added the slave op-amp configured as a simple inverter [see Fig. 3(b)]. As the master op-amp swings positive to its supply rail, the slave op-amp swings negative to its supply rail. This bridge configuration thus effectively doubles the compliance voltage, doubling the maximum load impedance that can be tolerated. The PA-85A op-amps (Apex μTechnologies; Tucson, AZ) used in our circuit allow us to achieve a compliance voltage of approximately 800 V in the bridge configuration.

The PA85A op-amps were selected for their unique combination of high-voltage tolerance (up to 450 V, rail to rail) and high slew rates (up to 1000 V/μs) using external compensation. Stability was optimized by using noninductively wound, high-voltage, metal-film, feedback resistors and by limiting the slew rate to 100 V/μs. The latter restriction still yielded rise times less than 2 μs since the load is largely capacitive at pulse onset.

Although the PA85A is a high-voltage op-amp, it is very sensitive to fault conditions and must be aggressively protected from noise and over-voltages at the power and input pins as well as from over-current conditions at the output. To protect the op-amps from power supply transients and over-voltages, decoupling capacitors were used in parallel with high-voltage tranzorbs (very fast, unidirectional zener diodes with sharp voltage break-over 'knees'). We used a parallel combination of three capacitor types to reduce power supply noise as much as possible over the entire bandwidth of the circuit. Four JFET's protect the inputs from large differential voltages, allowing a ±1.4-V maximum potential difference between the inverting and noninverting inputs. This potential difference is well within the safe range of ±25 V, while still providing enough of a differential voltage to drive the op-amp through its full linear range [32]. We chose JFET's based on their low gate capacitance, high input impedance and fast
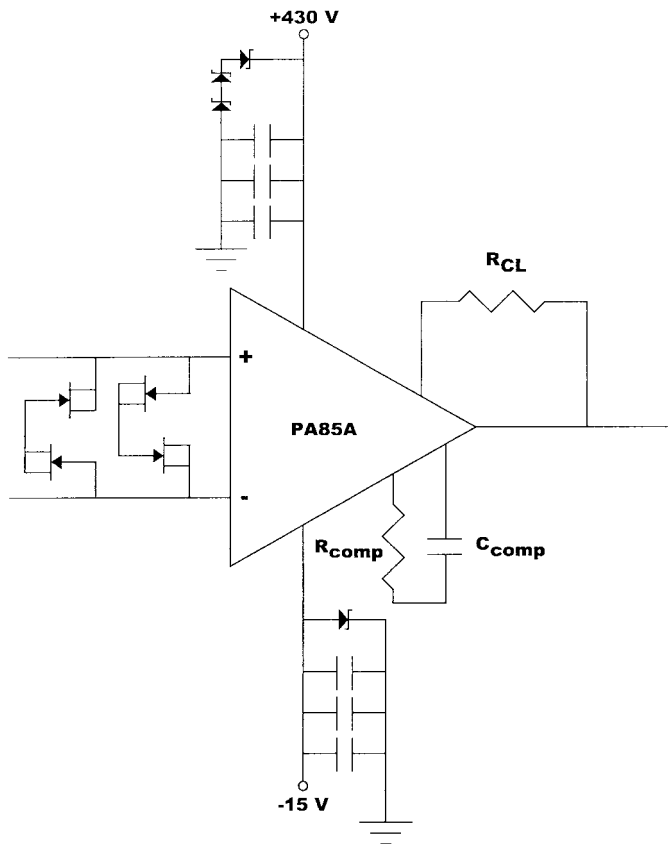
Fig. 4. Schematic showing master op-amp protection circuitry. JFET's are 2N5457. $R_{\text{comp}} = 100\ \Omega$, $C_{\text{comp}} = 75$ pF, R_{CL} (Current Limit) $= 8.3\ \Omega$.
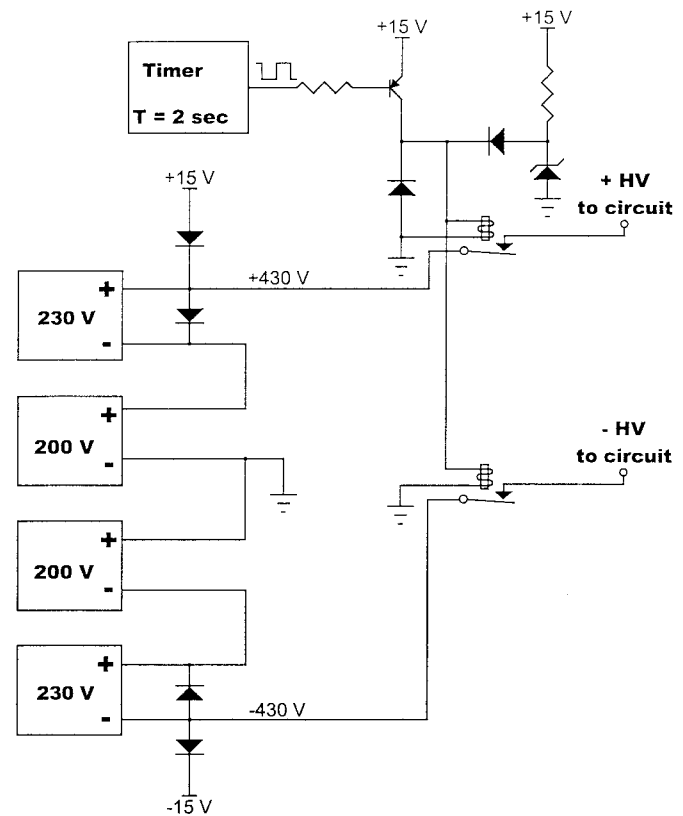

Fig. 5. The schematic of the high-voltage power management circuitry used to prevent common mode latch-up. Transformer-isolated, floating, high-voltage supplies are shown on the left. We avert common mode latch-up by using high-voltage relays to connect the ±430-V power supplies after a 1-s. delay generated by a timing circuit. Our design takes advantage of the hysteresis inherent in the relay solenoids to ensure that once the high-voltage power supplies are connected, they stay connected until the low-voltage power supplies go down.

switching speed. The op-amp protection circuitry is shown in Fig. 4.

B. Power Supply Management

One significant problem we experienced with our high-voltage design was "common mode latch-up." The stimulator output stage uses five power supply modules: one provides ±15 V; two 200-V and two 230-V floating supplies are stacked to provide ±430 V. The low-voltage supplies are able to source and sink far more current than the high-voltage supplies (1.5 A versus 0.1 A). The low-voltage supplies also settle much more quickly to their steady state values upon power up than do the high-voltage supplies. This is the root of the common mode latch-up problem. The master op-amp operates between supplies of +430 V and −15 V, while the slave op-amp operates between +15 V and −430 V (which is necessary so that 0 V is within the common mode range of the op-amps). If, at power-up, the power supplies were connected directly to the power pins of the op-amps, the low-voltage power supply would begin to source or sink current before the high-voltage supply would be ready to sink or source that current. The high-voltage power supply would be reverse biased and taken offline by its crowbar protection circuit. Thus, the ±15-V power would behave as expected, but the ±430-V power would be disabled. We avert common mode latch-up by using high-voltage relays to connect the ±430-V power

supplies after a 1-s delay generated by a timing circuit, as shown in Fig. 5. The high-voltage relays (DAT71210 Crydom Corporation, San Diego, CA) are initially open on power-up. After one second, the timer output goes high, applying 14.3 V to the relay coils, closing the relay contacts. After the timer output goes low again, the relays remain energized due to their inherent hysteresis and the zener diode. The zener voltage is midway between the relay's cut-in and cut-out voltages. The diodes near the power supplies prevent reverse bias of the high-voltage supplies and provide failsafe power to keep the op-amps from saturating in the event that any high-voltage supplies fail. This design has the added advantage of providing fail-safe protection to the subject by ensuring that if one of the low-voltage power supplies should fail, the high-voltage supplies are immediately removed from the circuit. In addition, it ensures that should an unexpected transient disrupt the high-voltage supply connection, the connection will be restored in an orderly manner within a second.

C. Input Stage

The input stage of the stimulator (Fig. 6) allows convenient and safe stimulation control by an external computer. Two identical optically coupled input channels allow sequential step
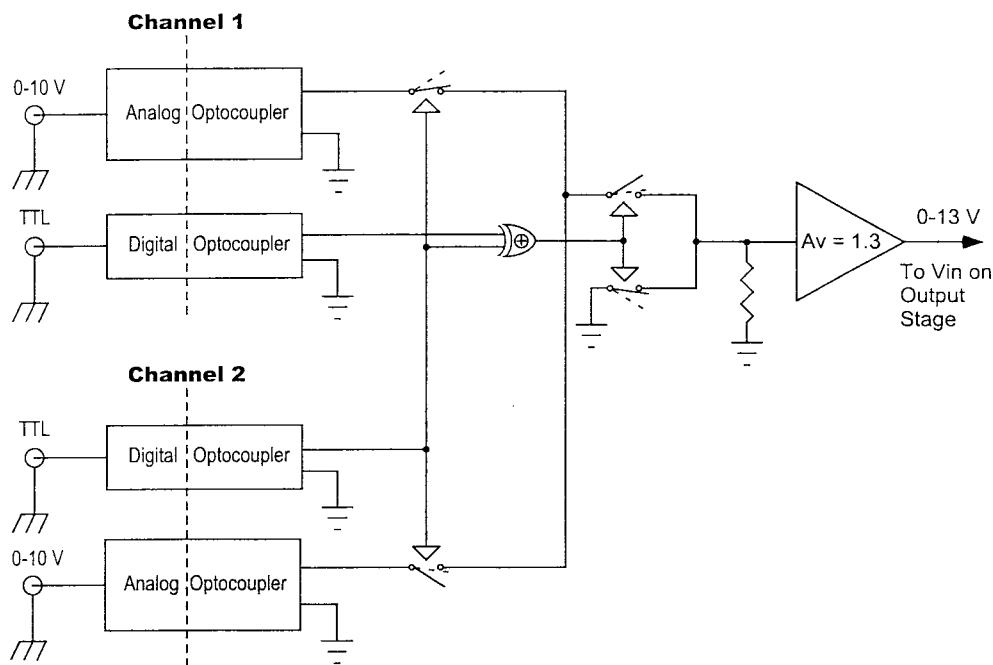
Fig. 6. The optically isolated input stage converts analog amplitude signals and digital timing signals into analog pulse waveforms used to control the stimulators output stage. Two identical channels are multiplexed to allow sequential step changes in current. Each channel has analog and digital portions to allow precise analog intensity control along with fast digital timing control. Fast TTL logic and solid state switches ensure that only one channel is active at a time. Components to the left of the dotted lines are powered relative to the controlling computer's ground, while those to the right are referenced to stimulator ground.

changes of current (e.g., a pulse of one amplitude and duration immediately followed by a pulse of different amplitude and duration) during the stimulus waveform. Each channel accepts two inputs: an analog (0–10 V) input controls stimulus intensity, and a digital (TTL level) input controls stimulus timing. This dual analog and digital control allows precise control of amplitude without sacrificing bandwidth and is similar to the isolation stage independently developed by Nohama *et al.* [34]. The stimulator input stage uses the TTL pulses to gate the analog input signals to produce the analog pulses that drive the output stage. The two channels are multiplexed to a single signal through TTL controlled analog switches. Logic circuitry ensures that only one channel has control of the output at any given time. Note that if neither input channel is active (or both are), then the drive to the output stage is grounded. The final op-amp of the input stage acts as a buffer, to ensure sufficient current drive to the output stage. This op-amp also provides a DC gain of 1.3 and frequency response tailored to avoid driving the output stage faster than it can slew.

The optical isolation of the analog signals is performed by high-linearity optocouplers (HCNR-200, Hewlett Packard; Palo Alto, CA) configured as precision analog isolation amplifiers (see HCNR200 technical data sheet [35, Fig. 17]. The input stage as a whole is linear to within 0.1%. The digital lines are optically isolated by high-speed digital optocouplers (HCPL-7100, Hewlett Packard; Palo Alto, CA).

D. Safety Considerations

Anytime high voltage comes in contact with human subjects, safety must be of primary concern. Our design incorporates many safety features intended to protect the subject from harmful electrical shock:

1) Power-Line Protection: All power supplies are transformer coupled and isolated from mains (AC) power via both an isolation transformer (XenTek EIT5706, isolation capacitance ≤ 0.001 pF) hardwired to the power cord and the isolation transformers in each of the individual power supplies (Power One, Inc. open frame linear supplies with insulation between supply frames and stimulator chassis). The stimulator chassis is hardwired to earth ground and leakage between any lead (or either high-voltage supply rail) to ground is less than 10 μA (as measured by a Dynatech Nevada Model PEI 2000B Digital Safety Analyzer), in accordance with hospital equipment safety standards [36]. This prevents the subject from being dangerously shocked if he or she touches a grounded appliance while being stimulated or in the unlikely event that a failure occurs and high-voltage power supplies are applied directly to the stimulating electrodes.

The optical isolation in the input stage ensures subject safety even if dangerous voltages are applied to the inputs.

2) Subject Setup/Subject Controlled Cut-Off Switch: The subject can completely disconnect himself from the stimulator by a switch hardwired to the stimulator cables, which can disconnect the subject leads and shunt the stimulator output through a low impedance load. In addition, the subject's finger is just resting on the cathode and the subject may pull it away in the event of painful shock.

*3) Measurement Techniques:* The electrode voltage is measured using a high-voltage, isolated probe (Tektronix A6902B) connected to a battery-powered oscilloscope (Hewlett Packard 54 601A with power inverter 85 901A). The current through the subject is measured by a clamp-on current probe (Tektronix AM 503A) around the stimulating leads, thereby maintaining electrical isolation between the subject and the AC power.
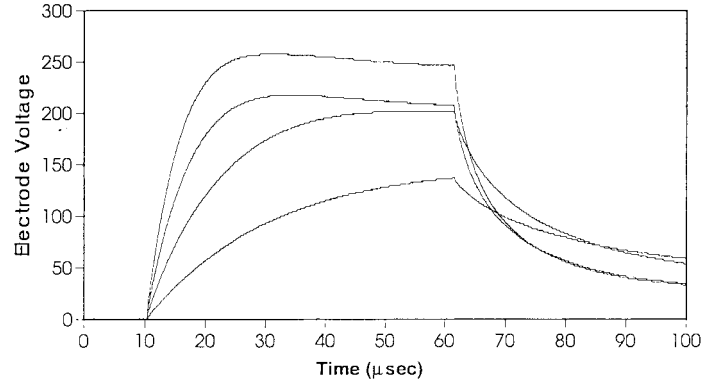
(a)
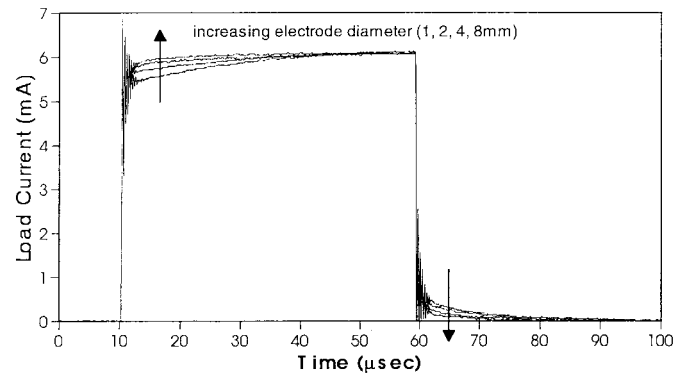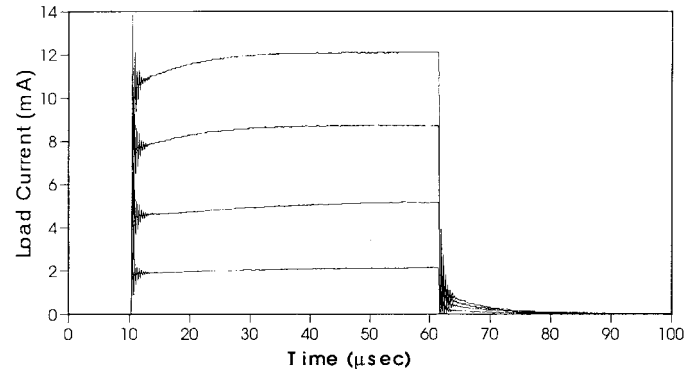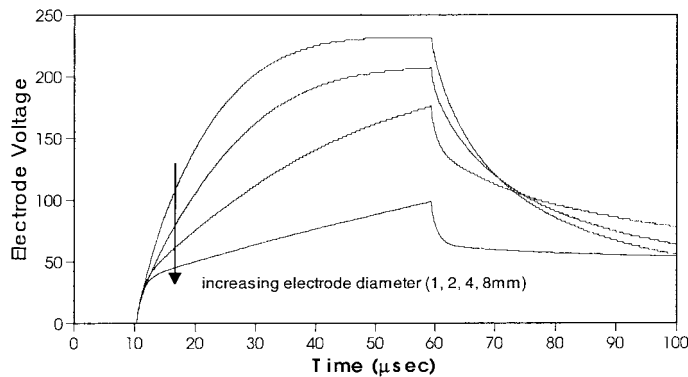
(b)

Fig. 7. Stimulus currents (a) and voltages (b) measured through 1-, 2-, 4-, and 8-mm-diameter electrodes placed on the volar tip of the third finger. The input to the stimulator was the same in all cases. Data were collected as described in the text, with each trace representing an average of 256 traces. Arrows indicate traces recorded from progressively increasing electrode diameter. Note that even though the surface area of the electrodes varied by a factor of sixteen, the current remained essentially unchanged.

4) Further Safety Issues: Note that we specifically wish to be able to pass DC current (for short periods of time, too short to cause tissue damage) as part of our research. If, however, one desired to limit the net DC current, one could easily modify the output stage by setting a slight negative offset on the master op-amp and connecting a 0.5 μF capacitor between the subject and the stimulator. This capacitor would allow a 25-mA pulse to flow for 1 ms, while decreasing the compliance voltage by only 50 V. At the same time, it would ensure that even in the event of stimulator failure, no more than 400 μC ($Q = C * V = 0.5$ μF $* 800$ V) of net charge could be transferred to the subject. This is less than the maximum safe charge, 520 μC, for cross-body surface stimulation [25].

III. RESULTS

The loads seen by the stimulator during electrocutaneous stimulation were highly nonlinear with respect to current. Figs. 7 and 8 display the results of tests performed using one subject's middle fingertip as the load; results from other subjects were not significantly different. Cathodic stimulation was delivered through four Ag/AgCl disk electrodes (1-, 2-, 4-, and 8-mm diameter) with a large, flexible electrode on the back of the finger serving as the anode. The pulses were each about

(a)

(b)

Fig. 8. Stimulus currents (a) and voltages (b) measured through a 1mm diameter electrode placed on the volar tip of the third finger. Data were collected as described in the text, with each trace representing an average of 256 traces.

50-μs long. Voltages and currents were measured as described above. Data traces were digitized to 8-bit accuracy by a digital scope after 256 waveforms were averaged to produce each trace. The resulting current measurement resolution was ±0.05 mA. Fig. 7(a) shows the actual current through the four electrodes for a constant input. Note that although the surface area of the electrode-skin interface varied by a factor of 16, the current output remained essentially unchanged. The corresponding stimulation voltages appear in Fig. 7(b). Fig. 8(a) and (b) shows the current and voltage waveforms measured by varying the current through the 1-mm-diameter electrode. Due to discomfort, 12 mA represented an upper bound for the stimulation currents in these tests (at this pulse width).

To assess the limits of the stimulator without the restrictions imposed by subject tolerance, we tested it using a wide variety of model loads built from discrete resistors and capacitors with values chosen to mimic the electrical impedance of the skin in various stimulation conditions. There were 24 models in all, each using the circuit shown in Fig. 1. Six values of R_p were used to span the observed physiological range (10, 20, 40, 80, 160, 320 kΩ). We used four values of C (0.42, 0.76, 1.7, 5.4 nF), each representing the estimated capacitance associated with one of the electrodes (1-, 2-, 4-, 8-mm, respectively). R_S was 2.2 kΩ in each case. Current and voltage waveforms were measured for each model while applying pulses of one

of three durations (25, 200, or 1000 μs) and three desired current levels (1, 5, or 25 mA). Waveforms were digitized for analysis after averaging 256 traces on the scope. In each case, the input waveform to the stimulator was adjusted to yield the desired current output through a 2 kΩ load (this is the minimum load for which this stimulator should be used). All of the model loads were then tested (at that nominal pulse width and current) without further input adjustments. Typical current and voltage waveforms were very similar to those shown for real fingers (Figs. 7 and 8), and were analyzed to compute rise time (10%–90%), percent initial overshoot, percentage of desired current achieved, and percent of ideal charge achieved. In each case, the rise time was less than 1 μs, with the majority under 300 ns. The overshoot varied, but was usually about 20%–25% of the steady state current. This overshoot is of no practical physiological importance since it is so brief (less than 1 μs) and, therefore, contains practically no charge. Our design represents a compromise between the desired fast rise and settling times and minimum overshoot and/or oscillation.

The applied current (and charge) was found to be within 5% of nominal in all cases except for the 25 μs, 1 mA pulses, where current was systematically too low by about 50 μA. In practice, this deviation could be reliably corrected through software calibration. The charge for all 1-mA pulses was likewise slightly out of the 5% tolerance as a result of the error in current. In the majority of cases, the charge and current were both within 1% of ideal. Note that in those cases where the load voltage reached the compliance voltage, the calculations were based only on the portion of the waveform occurring prior to the point at which the compliance voltage was reached. After the compliance voltage was reached, the current dropped to a lower level given by the compliance voltage divided by the real part of the load impedance (i.e., $R_p + R_S$). The time at which the current dropped due to the compliance voltage limitation was well predicted by a model assuming an ideal constant current source and fixed load component values. At the end of the nominal pulse, the current and voltage always returned to zero as desired. This is in contrast to the way some amplifiers fail to recover from saturation, with their outputs remaining high even after the input has been removed. This behavior would clearly not be desirable in a high-voltage stimulator, as it might result in large amounts of charge being transferred to the subject.

IV. DISCUSSION

We have developed a high-voltage electrocutaneous stimulator to aid in our investigation of the dynamic range of tactile fibers stimulated with small electrodes. We plan to use the stimulator to investigate the effects of stimulus waveform on pain and tactile thresholds as a function of electrode size. Our goal is to develop methods to increase the dynamic range available for stimulation through small electrodes. To quantify the effect of the stimulus waveform as well as geometric manipulations of the electrode surface, we will measure sensation and pain thresholds under a variety of conditions. The expected error of this type of threshold measure is about $\pm 5\%$, commensurate with the accuracy of the stimulator. The

accuracy of the device when delivering a specified charge is estimated to be $\pm 3\%$ on average, $\pm 1\%$ or better for 4 mm or larger electrodes. The accuracy with small electrodes could be improved through software calibration since the current is systematically about 50 μA too low.

The high-voltage design was necessary because of the high impedance of the skin and the use of electrodes with small surface areas. Conventional stimulators are not adequate for our purposes, since their compliance voltage is usually limited to less than 120 V [25]. Fig. 7 demonstrates that more than 220 V are required to apply a 6-mA pulse for 50 μs through a 1-mm-diameter electrode. The maximum compliance voltage of the present output stage is about 800 V. Unlike stimulators based on capacitive discharge [37], capacitive coupling or transformer coupling, the present stimulator is able to maintain the 800 Volts and up to 25-mA indefinitely, allowing the long (1 ms or longer) pulses we anticipate using in our experiments. The improved Howland current pump topology (with modifications for increased output impedance) was chosen to take advantage of the accuracy and speed given the available high-voltage op-amps. Current mirror configurations (e.g., [25]) were rejected due to the difficulty of finding the appropriate components with the necessary voltage ratings. Our first prototype was similar to the stimulator reported in [1] but could not be constructed with a sufficiently high compliance voltage using readily available components.

Because we anticipate the need to deliver very short pulses, we have designed the stimulator with fast rise times in mind. The result was that the stimulator's current output has a rise time below 2 μs (0.3 μs typical) for a square input pulse. This fast rise time came at the expense of adding significant overshoot (~25% for low impedance loads, less than 20% typical for physiological loads). This overshoot is so short, however, that it is of no physiological significance. If desired, the stimulator design could be modified so as to eliminate the overshoot by increasing the compensation on the output stage opamps. This increased compensation, however, will also increase the rise and settling times beyond that desired for our purposes.

We have chosen to design the stimulator for monophasic stimulation only. This type of stimulation is appropriate for use in a limited-time, laboratory application only. If one wished to use a high-voltage stimulator for longer-term stimulation, then some modifications would be needed to allow biphasic stimulation. There are several ways the design could be changed to allow biphasic (or at least charge balanced stimulation), but the way which preserves the greatest flexibility is as follows: 1) The input stage could be modified to allow both positive and negative excursions by configuring the optocouplers in a bipolar configuration as shown in Fig. 18 of the HCNR200 technical data sheets [35]. Alternately, one channel could be used for cathodic pulses and the other for anodic pulses. In this case, both inputs from the controlling computer could be positive going, but the anodic channel would simply be inverted in the optocoupling stage. This would involve very minimal changes to the input stage design, essentially just swapping inverting and noninverting terminals on a single op-amp. 2) The output stage would also need to be modified to

allow biphasic current swings. This would involve changing the supply rails on the PA85A op-amps to ±220 V each. This would allow equal cathodic and anodic currents and voltages. Note that this would limit the compliance voltage to approximately 400 V. These modifications could be combined with capacitive coupling (by placing a 0.5-μF capacitor in series with the load) to ensure limited net charge transfer even in the event of amplifier failure, while still allowing long (1 ms) pulses.

In summary, while we intend to use the high-voltage stimulator to investigate the effects of electrocutaneous stimulus waveforms on tactile sensations, the modifications we propose to the typical improved Howland current pump make our stimulator valuable in any application where a current controller is needed for high impedance loads. Likewise, the power management circuit presented should prove useful to others involved in high-voltage device design.

ACKNOWLEDGMENT

REFERENCES

[1] R. D. Melen and J. D. Meindl, "Electrocutaneous stimulation in a reading aid for the blind," *IEEE Trans. Biomed. Eng.*, vol. BME-18, pp. 1–3, 1971.
[2] C. C. Collins, "Electrotactile visual prosthesis," in *Functional Electrical Stimulation*, T. F. Hambrecht and J. B. Reswick, Eds.. New York: Marcel Dekker, 1977, p. 189.
[3] P. Bach-y-Rita, "Tactile vision substitution: Past and future," *Intern. J. Neurosci.*, 1983.
[4] K. Kaczmarek, P. Bach-y-Rita, W. J. Tompkins, and J. G. Webster, "A tactile vision-substitution system for the blind: Computer-controlled partial image sequencing," *IEEE Trans. Biomed. Eng.*, vol. BME-32, pp. 602–608, 1985.
[5] S. Tachi, K. Tanie, K. Komoriya, and M. Abe, "Electrocutaneous communication in a guide dog robot (MELDOG)," *IEEE Trans. Biomed. Eng.*, vol. BME-32, pp. 461–469, 1985.
[6] P. J. Blamey and G. M. Clark, "Psychophysical studies relevant to the design of a digital electrotactile speech processor," *JASA*, vol. 82, pp. 116–125, 1987.
[7] F. A. Saunders, "Recommeded procedures for electrocutaneous displays," in *Functional Electrical Stimulation*, T. F. Hambrecht and J. B. Reswick, Eds. New York: Marcel Dekker, 1977, p. 303.
[8] F. A. Saunders, "Electrotactile sensory aids for the handicapped," presented at 4th Annu. Meeting Biomedical Engineering Society, Los Angeles, CA, 1973.
[9] F. A. Saunders, "Electrocutaneous displays," presented at *Cutaneous Communication Systems and Devices Conf.*, Monterey, CA, 1974.
[10] T. A. Rohland, "Sensory feedback in upper-limb prosthetic systems," *Inter-Clin. Inform. Bull.*, vol. 13, pp. 1–8, 1974.
[11] H. Schmidl, "The importance of information feedback in prostheses for the upper limbs," *Prosth. Orthotics Int.*, vol. 1, pp. 21–24, 1977.
[12] G. F. Shannon, "A myoelectrically-controlled prosthesis with sensory feedback," *Med. Biol. Eng. Comput.*, vol. 17, pp. 73–80, 1979.
[13] R. E. Prior, J. L. Lyman, P. A. Case, and C. M. Scott, "Supplemental sensory feedback for the VA/NU myoelectric hand. Background and preliminary designs," *Bull. Prosth. Res.*, vol. 11, pp. 171–191, 1976.
[14] R. N. Scott, R. H. Brittain, R. R. Caldwell, A. B. Cameron, and V. A. Dunfield, "Sensory-feedback system compatible with myoelectric control," *Med. Biol. Eng. Comput.*, vol. 18, pp. 65–69, 1980.
[15] R. H. Scott, "Feedback in myoelectric prostheses," *Clin. Orth. Related Res.*, vol. 256, pp. 58–63, 1990.
[16] D. F. Lovely, B. S. Hudgins, and R. N. Scott, "Implantable myoelectric control system with sensory feedback," *Med. Biol. Eng. Comput.*, vol. 23, pp. 87–89, 1985.
[17] R. E. Prior, P. A. Case, and J. Lyman, "Supplemental sensory feedback for the below elbow amputee," presented at 29th ACEMB Conf., Boston, MA, 1976.
[18] A. Y. J. Szeto and J. Lyman, "Comparison of codes for sensory feedback using electrocutaneous tracking," *Ann. Biomed. Eng.*, vol. 5, pp. 367–383, 1977.
[19] J. Kawamura, O. Sueda, K. Harada, K. Nishihara, and S. Isobe, "Sensory feedback systems for the lower-limb prosthesis," *J. Osaka Rosai Hospital*, vol. 5, pp. 104–112, 1981.
[20] J. A. Sabolich and G. M. Ortega, "Sense of feel for lower-limb amputees: A phase-one study," *J. Prosth. Orthotics*, vol. 6, pp. 36–41, 1994.
[21] H. P. Schmid and G. A. Bekey, "Tactile information processing by human operators in control systems," *IEEE Trans. Syst. Man Cybern.*, vol. SMC-8, p. 860, 1978.
[22] R. R. Riso, A. R. Ignagni, and M. W. Keith, "Cognitive feedback for use with FES upper extremity neuroprostheses," *IEEE Trans. Biomed. Eng.*, vol. 38, pp. 29–38, 1991.
[23] C. C. Collins and J. M. J. Madey, "Tactile sensory replacement," in *Proc. San Diego Biomed. Symp.*, 1974, vol. 13, pp. 15–26.
[24] K. A. Kaczmarek, J. G. Webster, P. Bach-y-Rita, and W. J. Tompkins, "Electrotactile and vibrotactile displays for sensory substitution systems," *IEEE Trans. Biomed. Eng.*, vol. 38, pp. 1–16, 1991.
[25] K. A. Kaczmarek, K. M. Kramer, J. G. Webster, and R. G. Radwin, "A 16-channel 8-parameter waveform electrotactile stimulation system," *IEEE Trans. Biomed. Eng.*, vol. 38, pp. 933–943, 1991.
[26] A. M. Kligman, "The biology of the stratum corneum," in *The Epidermis*, W. Montagna and J. W. C. Lobitz, Eds. New York: Academic, 1964, pp. 387–433.
[27] D. T. Lykken, "Square-wave analysis of skin impedance," *Psychophysiol.*, vol. 7, pp. 262–275, 1970.
[28] M. Reichmanis, A. A. Marino, and R. O. Becker, "Electrical correlates of acupuncture points," *IEEE Trans. Biomed. Eng.*, vol. BME-22, pp. 533–535, 1975.
[29] C. E. Burton, R. M. David, W. M. Portnoy, and L. A. Akers, "The application of Bode analysis to skin impedance," *Psychophysiol.*, vol. 11, pp. 517–525, 1974.
[30] R. Edelberg, "Electrical properties of the skin," in *Biophysical Properties of the Skin*, H. R. Elden, Ed. New York: Wiley, 1971, p. 513.
[31] A. Y. J. Szeto and R. R. Riso, *Sensory Feedback Using Electrical Stimulation of the Tactile Sense*. Boca Raton, FL: CRC, 1990.
[32] *Apex Data Book*, vol. 8, Apex Microtechnology Corporation, Tucson, AZ, 1998.
[33] P. Horowitz and W. Hill, *The Art of Electronics*, 2nd ed. Cambridge, U.K.: Cambridge Univ. Press, 1991.
[34] P. Nohama and A. Cliquet Jr., "A solution for linearity, stability and frequency bandwidth in PAM electrocutaneous stimulators' isolation interface," *Med. Eng. Phys.*, vol. 18, pp. 692–695, 1996.
[35] "HCNR200 datasheets," in *Isolation and Control Designers Catalog, Components*. San Jose, CA: Hewlett Packard Corp., pp. 5865–6008E, 1996.
[36] NFPA 99 Standard for Health Care Facilities, Dallas, TX: NFPA, 1993.
[37] J. B. Reilly and W. D. Larkin, "Electrocutaneous stimulation with high-voltage capacitive discharges," *IEEE Trans. Biomed. Eng.*, vol. BME-30, pp. 631–641, 1983.

Christopher J. Poletto received the B.S. degree in electrical engineering from Rice University, Houston, TX, in 1990 and the M.S. degree in biomedical engineering from Case Western Reserve University (CWRU), Cleveland, OH, in 1995. He is currently pursuing the Ph.D. degree at CWRU.

From 1990 to 1993, he worked in West Africa for Schlumberger International as an oil well data logging engineer and analyst (Senior Field Engineer). His research interests include mathematical modeling of excitable tissues, sensory substitution, functional electrical stimulation, and rehabilitation engineering.

Clayton L. Van Doren received the B.S. degree in physics from Case Western Reserve University (CWRU), Cleveland, OH, in 1980 and the Ph.D. degree in neuroscience from Syracuse University, Syracuse, NY, in 1987.

Since 1987, he has worked in the Departments of Orthopaedics and Biomedical Engineering at Case Western Reserve University and is currently an Assistant Professor of Orthopaedics at CWRU. His research interests are in the sensory and motor functions of the hand, including sensory substitution for kinesthetic and cutaneous modalities.